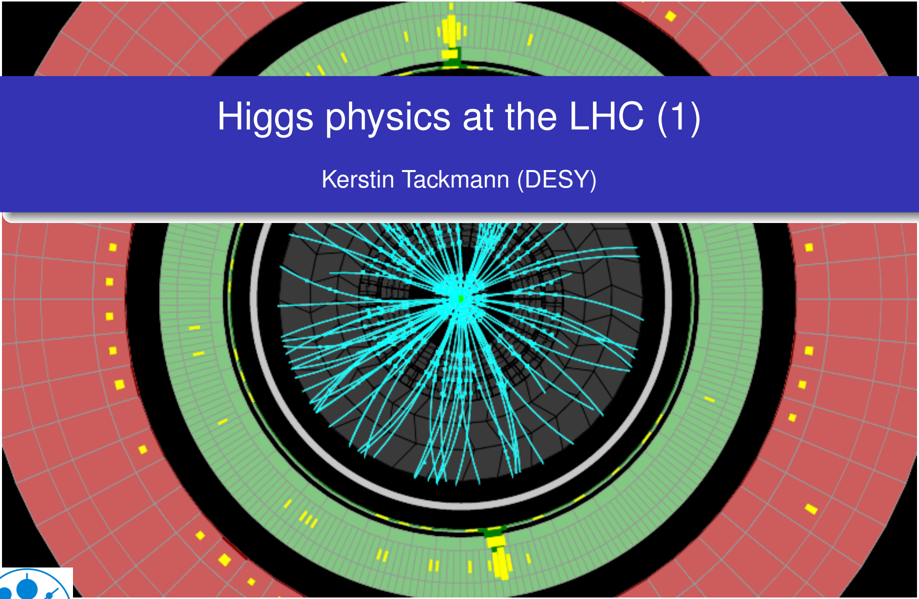

Higgs physics at the LHC (1)

Kerstin Tackmann (DESY)

PRISMA/Symmetry Breaking Annual Retreat 2017

Outline

Topics of the lectures

- Overview LHC, proton collisions, and the experiments
- The Higgs boson in the SM
- A close look at the $H \to \gamma\gamma$ analysis: analysis techniques
- Overview of Higgs measurements and searches in other decay channels and combined results

General remarks

- Please interrupt to ask questions!
- In many cases I will use ATLAS examples, but most measurements and searches are done by both CMS and ATLAS

Many thanks to Peter Jenni, Andreas Hoecker, Sandra Kortner, Manuella Vincter, Giacinto Piacquadio, and Witold Kozanecki for material used in these slides.

Why a hadron collider?

Energy loss from synchrotron radiation in a circular collider (per turn)

$$\Delta E = \frac{q^2}{3R\epsilon_0}\left(\frac{E}{mc^2}\right)^4 \qquad \frac{\Delta E_e}{\Delta E_p} = \left(\frac{m_p}{m_e}\right)^4 \sim 10^{13}$$

$\rightarrow$ Higher energies much easier to reach with proton collisions

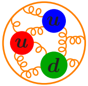

But protons also have disadvantages ...

- ...only part of the protons' energies is available for the partonic collision
- ...unkown boost along the beam direction (incomplete kinematic information)
- ...large probability for low-energy processes
- ...strong interaction makes theoretical predictions more complicated

Large Hadron Collider (@CERN, Geneva)

LHC uses LEP tunnel

- Circumference $\sim$ 26.7 km
- $\sim$ 100 m below the surface

Design: pp collisions at $\sqrt{s} = 14$ TeV

pp collisions at

- 2009 $\sqrt{s} = 900$ GeV
- 2010/11 $\sqrt{s} = 7$ TeV
- 2012 $\sqrt{s} = 8$ TeV
- 2015-17 $\sqrt{s} = 13$ TeV

- 2013/14 shutdown: machine and detector consolidation

in addition p-lead and lead-lead collisions

The LHC (pre-)accelerator chain

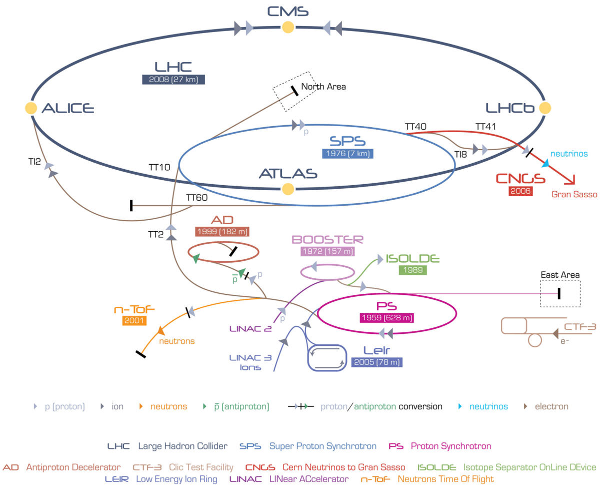

Linac 60 MeV

Booster 1.4 GeV

PS 25 GeV

SPS 450 GeV

LHC 3.5-7 TeV

>50 years of CERN history still operational

Previous main accelerator turns into pre-accelerator for the next step

LHC design parameters

beam energy	7	TeV
instantaneous luminosity	10^{34}	$cm^{-2}s^{-1}$
integrated luminosity/year	~ 100	fb^{-1}
dipole field	8.4	T
dipole current	11700	A
circulating current/beam	0.53	A
number of bunches	2808	
bunch spacing	25	ns
protons per bunch	10^{11}	
rms beam radius at IP1/5	16	μm
rms bunch length	7.5	cm
stored beam energy	360	MJ
crossing angle	300	μrad
number of events per crossing	20	
luminosity lifetime	10	h

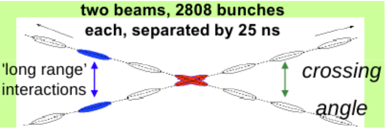

...but this is not how LHC has been operating so far

Beam energy stored in each LHC beam 360 MJ

Equivalent to

- Kinetic energy: 450 cars at 100 km/h
- Chemical energy: 70 kg of chocolate

Luminosity and event rate

Rate of events N produced for a process with cross section σ

$$dN/dt = \mathcal{L}\sigma$$

Luminosity depends on the beam parameters

$$\mathcal{L} = \frac{N_p^2 n_{\mathrm{bunch}} f}{A}$$

with

- N_p number of protons/bunch (10^{11})
- n_{bunch} number of bunches (2808)
- f revolving frequency (11245 Hz)
- A effective cross section area of beams

Integrated luminosity

$$L = \int \mathcal{L} dt$$

Instantaneous luminosity at LHC

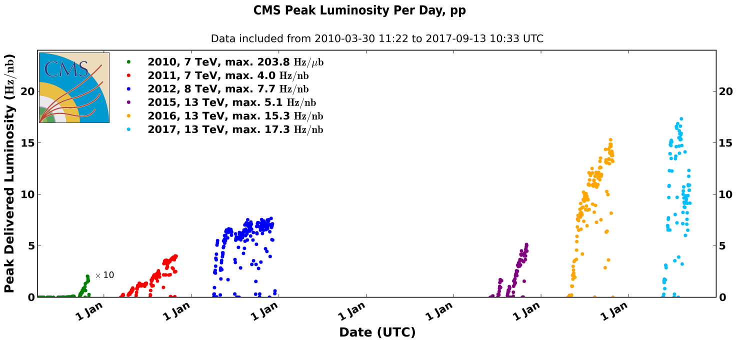

- Significant increase of instantaneous luminosity over time
  - ⋆ Increase of number of bunches, protons per bunch, more tightly focused beam
  - ⋆ Operation with 25 ns bunch spacing since summer 2015
- Design instantaneous of $1 \times 10^{34}\,\mathrm{cm}^{-2}\,\mathrm{s}^{-1}$ surpassed in summer 2016

Integrated luminosity

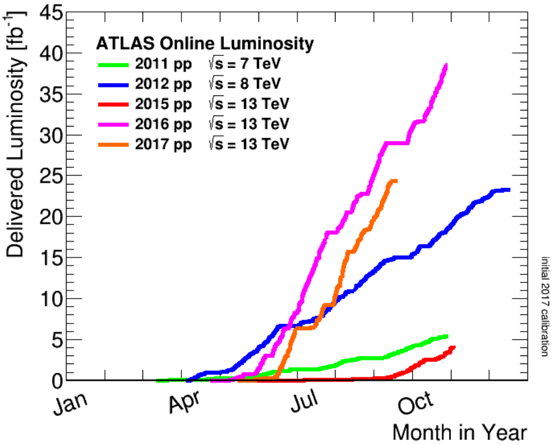

2016	38.5 fb^{-1}
2012	23.3 fb^{-1}
2017	24.3 fb^{-1}
2011	5.6 fb^{-1}
2015	4.2 fb^{-1}
2010	0.048 fb^{-1}

- In most years LHC has outperformed expectations
  - ⋆ E.g. at the beginning of 2011, we were hoping for ∼1 fb^{-1}
- Efficiency (delivered by LHC → analyzed) ∼90%

Total pp cross section

- Total pp cross section $\sigma_{\text{tot}} = \sigma_{\text{elastic}} + \sigma_{\text{inelastic}}$
- Inelastic term can be decomposed as
  $\sigma_{\text{inelastic}} = \sigma_{\text{single diffractive}} + \sigma_{\text{double diffractive}} + \sigma_{\text{non-diffractive}}$

- Single (double) diffractive: $pp \to pX(XX)$, clear gap
- Non-diffractive: $pp \to X$, gaps filled by particles

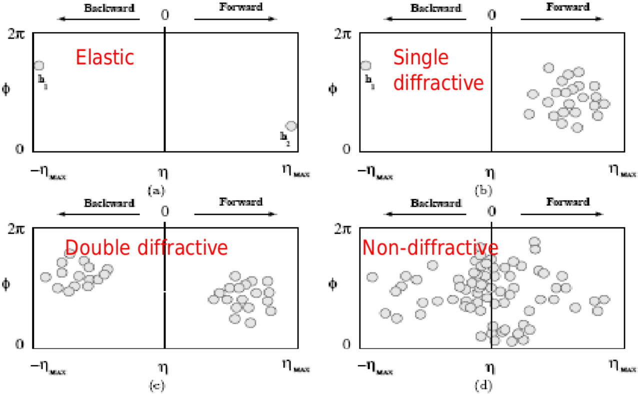

Inelastic collisions per bunch crossing

- Number of inelastic collisions per bunch crossing

$$< \mu >= \sigma_{\text{inel}} \ \mathcal{L} \ \Delta t \ / \ \epsilon^{\text{occupancy}}_{\text{bunch}}$$

- LHC $< \mu >=\sim 80\,\text{mb}\ 10^{34}\,\text{cm}^{-2}\,\text{s}^{-1}\ 25\,\text{ns}\ /\ 0.8 = 20 - 25$
  - ⋆ On average, $>$20 simultaneous pp collisions per bunch crossing
- Much more than at recent machines
  - ⋆ LEP $\Delta t = 22\,\text{ms}$ and $< \mu > << 1$
  - ⋆ SppS $\Delta t = 3.3\,\text{ms}$ and $< \mu > \approx 3$
  - ⋆ HERA $\Delta t = 96\,\text{ns}$ and $< \mu > << 1$
  - ⋆ Tevatron $\Delta t = 0.4\,\text{ms}$ and $< \mu > \approx 2$

The price of high luminosity: many events overlayed in the detector

ATLAS was designed to operate with 23 interactions overlayed

Proton collisions are a bit messy...

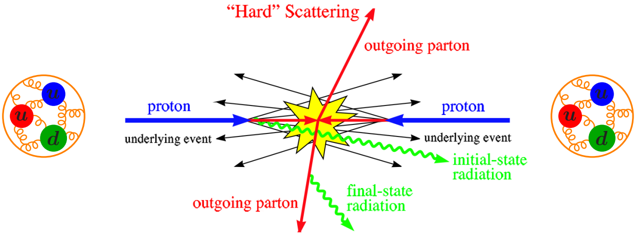

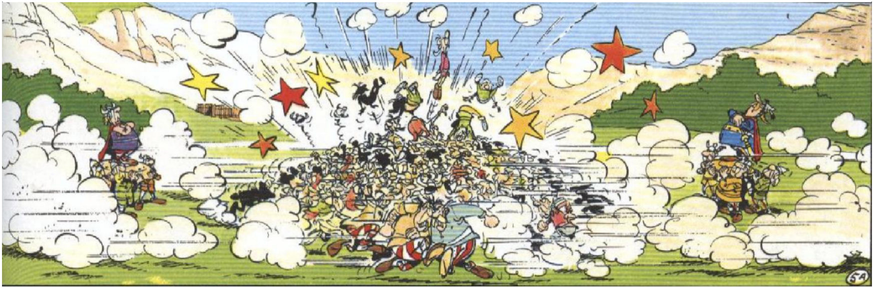

Proton collisions in detail...

...or rather, how we simulate them...

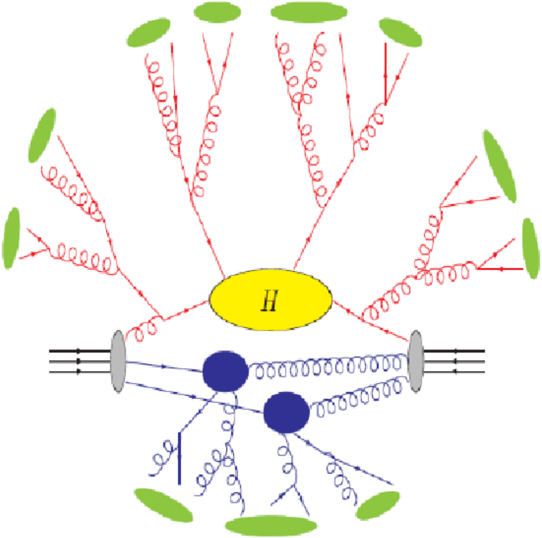

+ Decay

Hadronization of partons to hadrons, nonperturbative model

Parton shower: splitting of partons $\rightarrow$ modeling initial and final state radiation

Hard scatter described by matrix element (perturbative)

Proton structure: partons inside the proton

Multiple parton interactions: interactions of remaining partons in protons

Cross sections

Cross section (σ) is the probability that a process $a + b \rightarrow X$ occurs when a and b collide

- Differential cross section $\mathrm{d}\sigma/\mathrm{d}y$ is the probability for final state with given $\mathrm{d}y$
  - ⋆ Example: jet transverse momentum spectrum $\mathrm{d}\sigma/\mathrm{d}p_T$

Proton collisions: For inclusive processes $\sigma(pp \rightarrow X)$ can be computed via factorization theorem, separating the short distance and long distance

$$\sigma_{pp\rightarrow X} = \sum_{a,b} \int_0^1 \mathrm{d}x_1 \mathrm{d}x_2 f_a(x_1, Q^2) f_b(x_2, Q^2) \hat{\sigma}_{ab\rightarrow X}(x_1, x_2, Q^2)$$

- ⋆ Hard scattering: production of W, Z, top, Higgs, ..., computed in perturbative QCD at scale Q^2
- ⋆ Parton distribution functions → nonperturbative structure of the proton

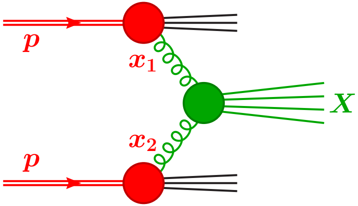

Note: strictly speaking only proven for inclusive processes

Parton distribution functions (pdfs)

- Proton content: valence quarks, sea quarks, gluons
- Momentum distribution of partons described by pdfs, function of
  - ⋆ Momentum fraction (of proton momentum) x
  - ⋆ Q^2 (scale of hard process)
- CM energy for parton collision $\hat{s} = x_1 x_2 s (= m_X^2)$
- For $m_X = 100\,\mathrm{GeV}$
  - ⋆ Tevatron ($\sqrt{s} = 2\,\mathrm{TeV}$) $x = 0.22$ (if $x_1 = x_2$)
  - ⋆ LHC ($\sqrt{s} = 14\,\mathrm{TeV}$) $x = 0.08$ (if $x_1 = x_2$)

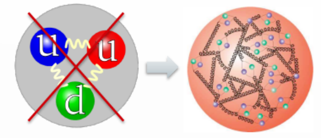

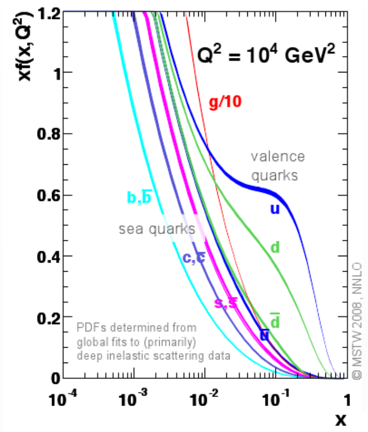

→ Larger cross sections at LHC

→ LHC: cross section dominated by gg

Production cross sections at hadron colliders

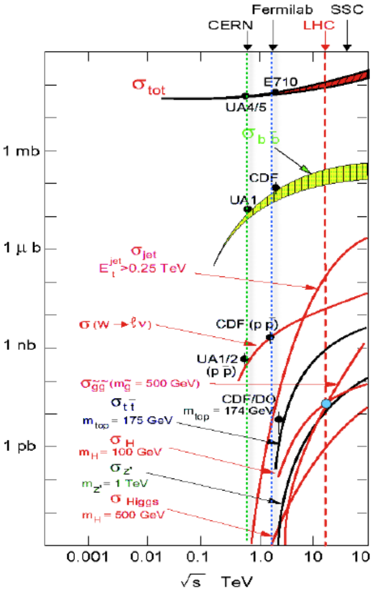

Process	Cross section (nb) at 14 TeV CM energy	Production rates (Hz) at $L=10^{34}$ cm^{-2}s^{-2}
Inelastic	10^8	10^9
$b\bar{b}$	5×10^5	5×10^6
$W \to \ell\nu$	15	150
$Z \to \ell\ell$	2	20
$t\bar{t}$	1	10
Z' (1 TeV)	0.05	0.5
$\tilde{g}\tilde{g}$ (1 TeV)	0.05	0.5
H (120 GeV)	0.04	0.4
H (180 GeV)	0.02	0.2

Many orders of magnitude between Higgs/New Physics and QCD backgrounds

Minimum bias events

- “Any inelastic non-diffractive event” or “A generic pp inelastic non-diffractive event”
- Experimentally “anything that triggers the minimum bias trigger”
  - ⋆ This is effectively any non-single diffractive (nsd) inelastic event

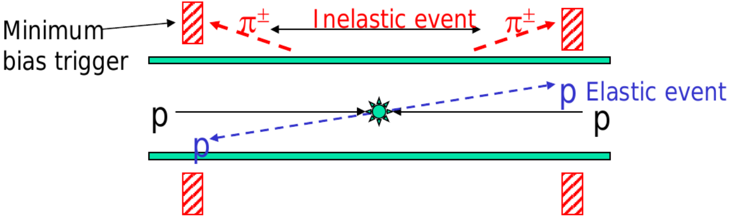

- Minimum bias cross section fills almost the total inelastic cross section ($\sigma_{\text{inel}} = 80 - 85\,\text{mb}$, $\sigma_{\text{nsd}} = 65 - 70\,\text{mb}$)
- Mainly soft QCD interactions
- (Almost) all (additional) pp interactions in a recorded pp event are minimum bias events

Pileup

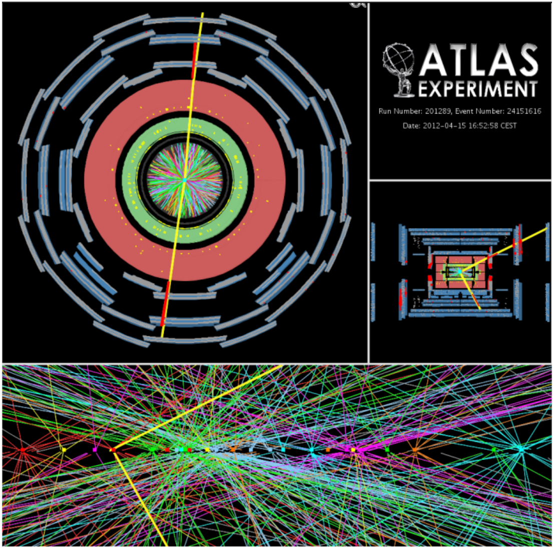

$Z \to \mu\mu$ with 25 interaction vertices

Challenge to trigger, software and analyses

- $\rightarrow$ Large amount of data to process and store
- $\rightarrow$ Identification and measurement of the "interesting" objects

Especially for jets, E_T^{miss} and τ

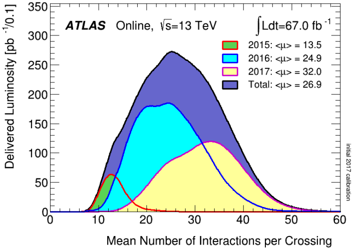

In-time and out-of-time pileup

In-time

- Additional pp collisions occuring in the same bunch crossing as the collision of interest
- Can be suppressed by identifying pp collision vertex of interest

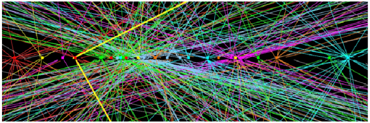

Out-of-time

- Additional pp collisions occuring in bunch crossings (just) before and after the collision of interest
- Typically corrected for on average
- E.g. ATLAS LAr calorimeter detector pulse $\sim$450 ns
- Shaped by electronics such that average net contribution of in- and out-of-time pileup cancel for design running conditions

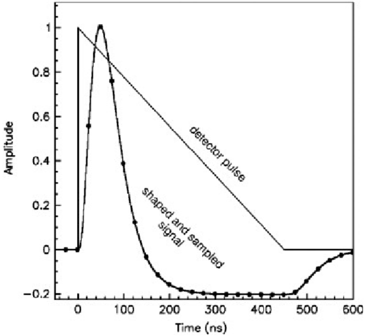

Kinematic variables

Transverse momentum p_T and missing transverse momentum "E_T^{miss}"

- Transverse momentum is conserved $\sum \vec{p}_T^{\,i} = 0$
- Large missing transverse momentum $E_T^{\mathrm{miss}} = |\vec{p}_T^{\,\mathrm{miss}}| \rightarrow$ invisible particle escaped detection (e.g. neutrino)

Longitudinal momentum p_z and (visible) energy E

- Boost of partonic CM unknown $\rightarrow$ cannot use p_z and E conservation

Polar angle θ

- Not Lorentz invariant

Pseudorapidity η and rapidity y

$$\eta = \frac{1}{2}\ln\frac{|\vec{p}| + p_z}{|\vec{p}| - p_z} = -\ln\left(\tan\frac{\theta}{2}\right) \; (= y \text{ if } m = 0)$$

$$y = \frac{1}{2}\ln\frac{E + p_z}{E - p_z} = \frac{1}{2}\ln\frac{x_1}{x_2}$$

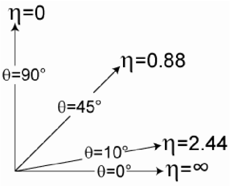

- Δy and p_T are invariant under longitudinal boosts
- Particle production in hadron colliders is roughly constant in y

ATLAS

- 2 T solenoid magnet
- Tracking: Si pixel, microstrip, straw tubes
- Transition radiation for $e^{\pm}$ id
- Pb/LAr and steel/scint, Cu/LAr calos
- μ chambers in $\sim$0.4 T toroid field

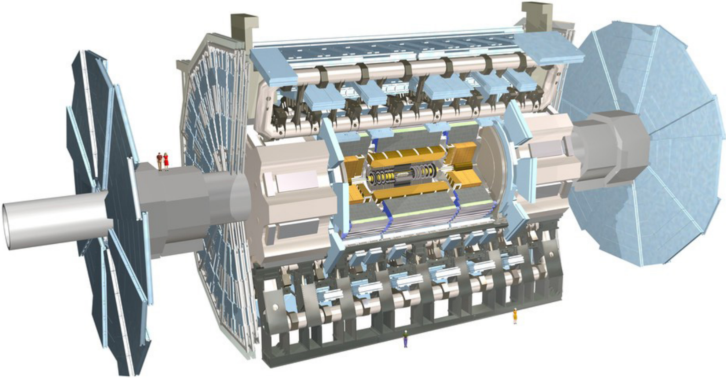

24 m$\times$45 m
7 ktons

ATLAS inner detector ($|\eta| < 2.5$)

Pixel detector

- 4 barrel layers, 2×3 endcap disks
- Innermost layer (IBL) installed for Run2 (33 mm radius)
- Pitch 50 μm × 400 μm (250 μm for IBL)

Silicon microstrip detector (SCT)

- 4 barrel layers, 2×9 endcap disks
- Pitch 80 μm, 40 mrad stereo angle

Transition radiation tracker

- Typically 36 straw-tube hits per track
- Transition radiation in scintillators to identify electrons

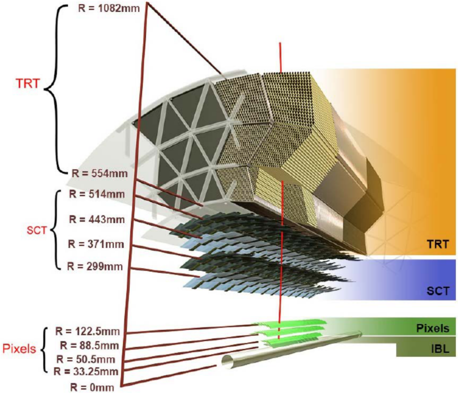

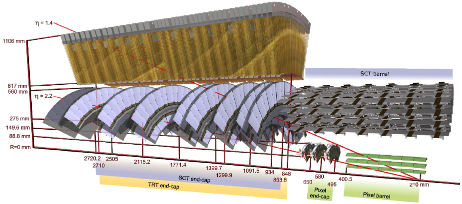

ATLAS calorimeters

Electromagnetic calo ($|\eta| < 3.2$)

- Pb/LAr sampling calorimeter
- Radiation hard
- 3 longitudinal layers with accordion geometry and presampler inside of cryostat
- Fine lateral segmentation $\rightarrow$ measure shower shape

Hadronic calo

- Iron/plastic scintillator tiles sampling calorimeter ($|\eta| < 1.7$)
- Copper (EC) and tungsten (FCal)/LAr sampling calorimeter ($|\eta| < 4.9$)

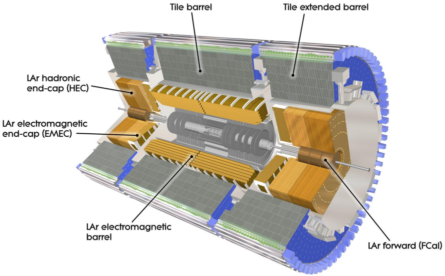

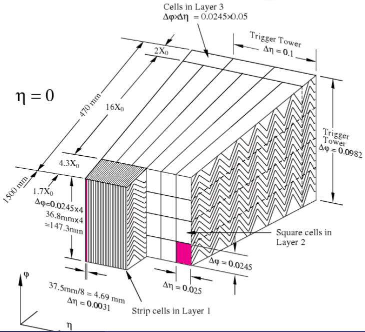

ATLAS muon spectrometer ($|\eta| < 2.7$)

- 3 barrel layers, 2$\times$3 endcap wheels
- Fast trigger chambers: TGC (thin gap chambers), RPC (resistive plate chambers)
- High resolution tracking: MDT (monitored drift tubes), CSC (cathode strip chambers)
- Air-core toroids ($< B >= 0.4\,\mathrm{T}$)
  - ⋆ Large field variations in toroid, close to 4 T near coil

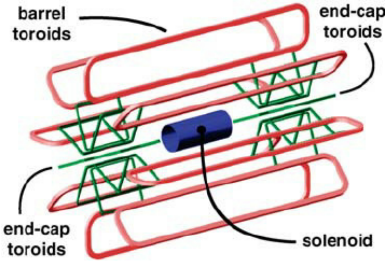

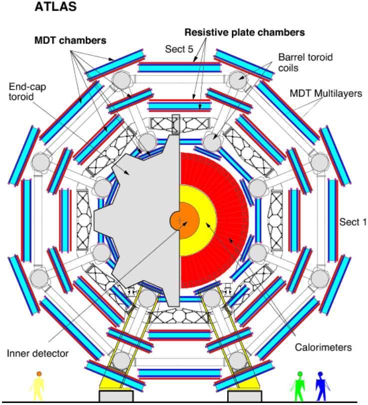

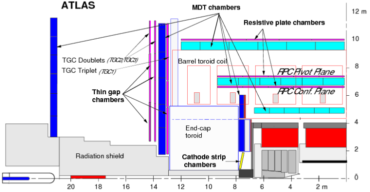

CMS

- 4 T solenoid magnet
- Tracking: Si pixel, microstrip
- $PbWO_4$ crystals and Fe/scint calos
- μ chambers in return yoke

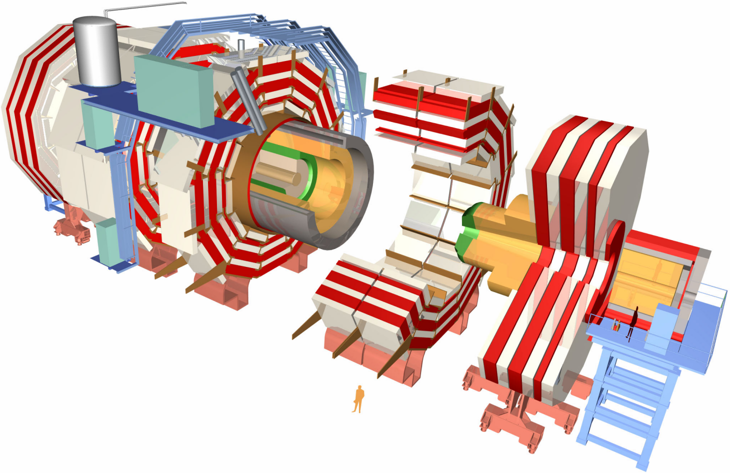

15 m$\times$22 m
12.5 ktons

Object reconstruction

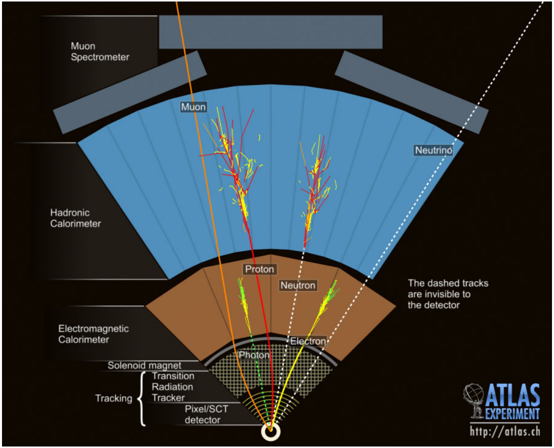

Electron

- Track in tracking system
- Shower in electromagnetic calorimeter
- No (or little) energy in hadronic calorimeter

Object reconstruction

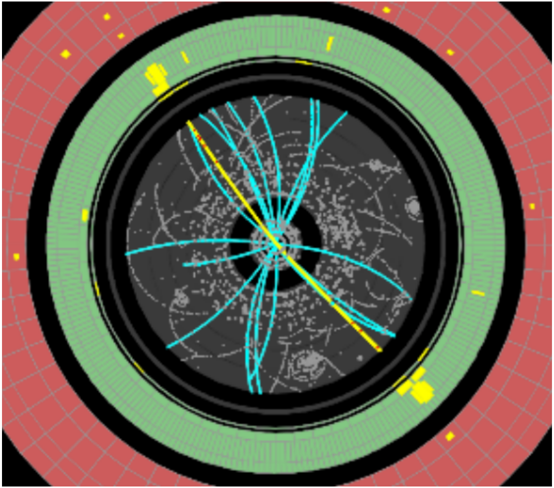

Electron

- Track in tracking system
- Shower in electromagnetic calorimeter
- No (or little) energy in hadronic calorimeter

Object reconstruction

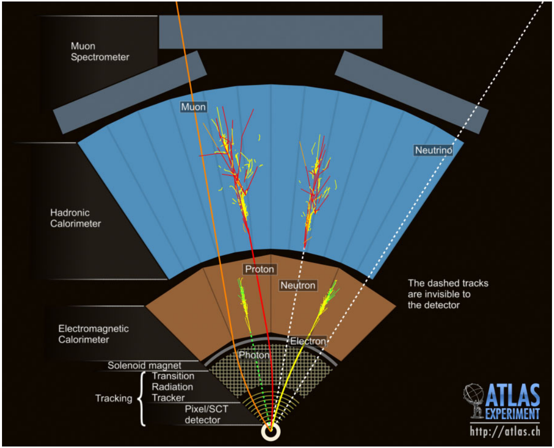

Photon

- No track or conversion vertex in tracking system
  - ⋆ $\sim$40% of photons convert into e^+e^- due to high material budget
- Shower in electromagnetic calorimeter
- No (or little) energy in hadronic calorimeter

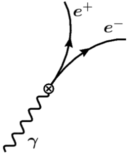

Object reconstruction

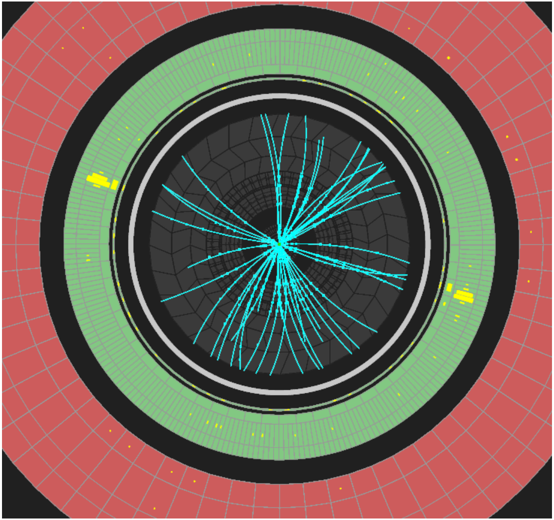

Photon

- No track or conversion vertex in tracking system
  - ⋆ ∼40% of photons convert into e^+e^- due to high material budget
- Shower in electromagnetic calorimeter
- No (or little) energy in hadronic calorimeter

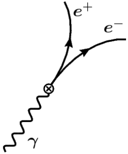

Object reconstruction

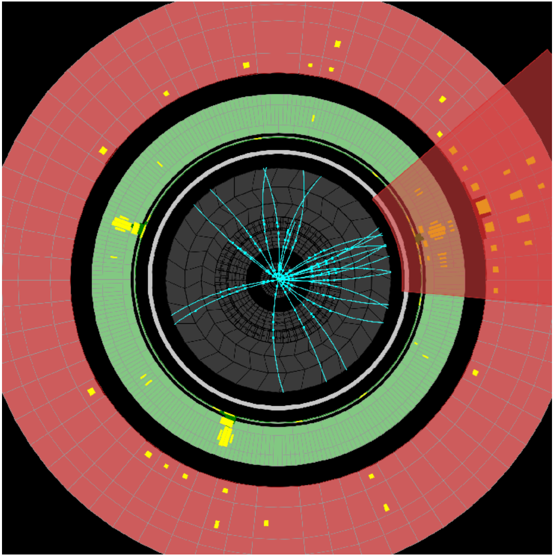

Hadron (Jet = hadronic shower)

- Tracks in tracking system (from charged component)
- Shower in hadronic and electromagnetic calorimeter

Object reconstruction

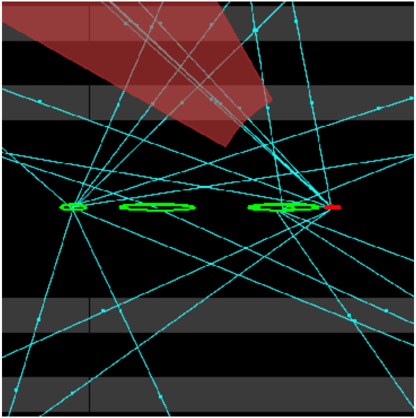

Hadron (Jet = hadronic shower)

- Tracks in tracking system (from charged component)
- Shower in hadronic and electromagnetic calorimeter

Object reconstruction

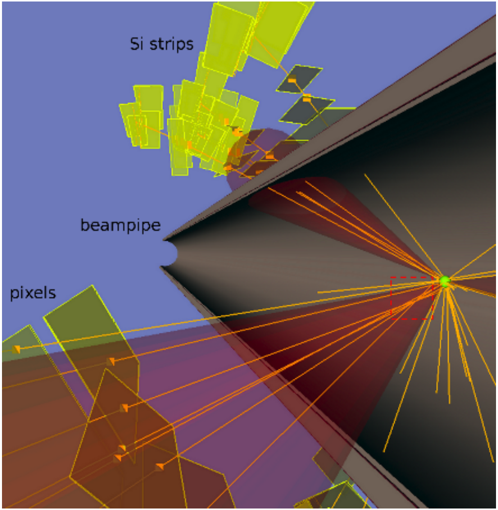

Hadron (Jet = hadronic shower)

- Tracks in tracking system (from charged component)
- Shower in hadronic and electromagnetic calorimeter

b-jet

- Origin of tracks offset with respect to pp interaction vertex

Object reconstruction

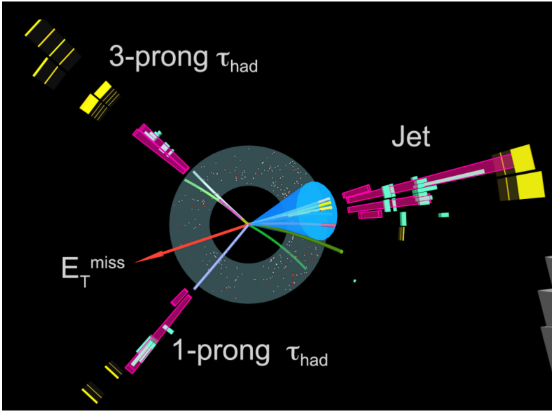

τ

- Hadronic (τ-jet):
  Collimated, 1 or 3 tracks in tracking system
- Leptonic ($\tau \to e(\mu)\nu\nu$):
  1 track: electron or muon

Object reconstruction

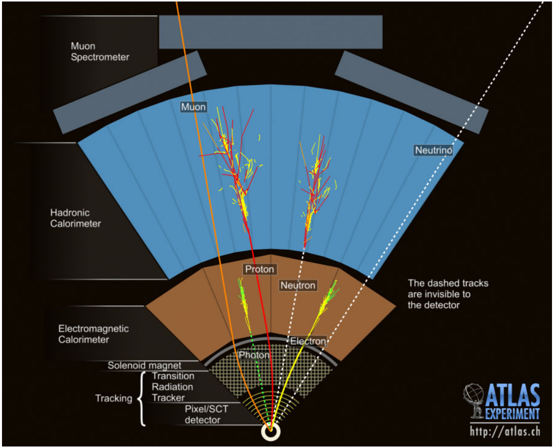

Muon

- Track in tracking system
- Little energy deposited in electromagnetic calorimeter
- Track in muon system

Object reconstruction

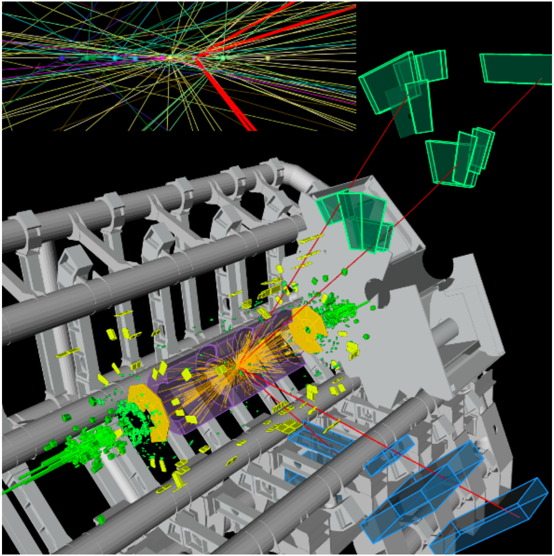

Muon

- Track in tracking system
- Little energy deposited in electromagnetic calorimeter
- Track in muon system

Object reconstruction

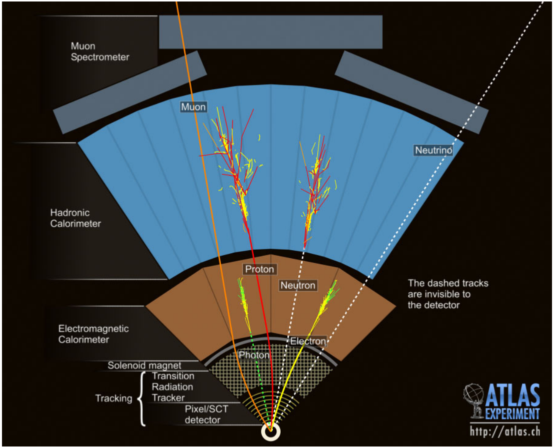

Neutrino (E_T^{miss})

- No signal in any subdetector
- Transverse energy imbalance in the event

Object reconstruction

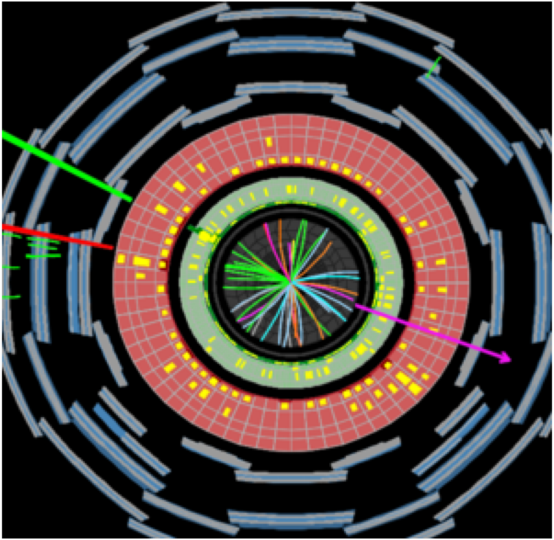

Neutrino (E_T^{miss})

- No signal in any subdetector
- Transverse energy imbalance in the event

The ATLAS and CMS experiments – comparison

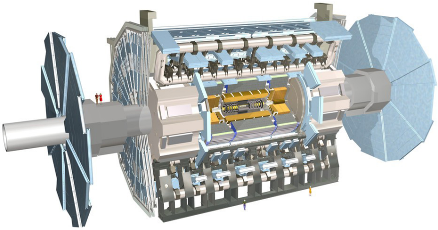

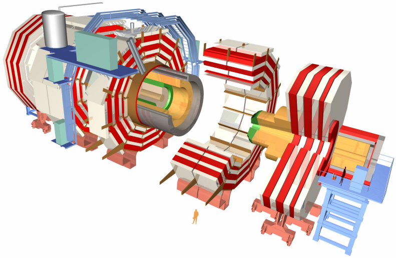

ATLAS Emphasis on jet and missing E_T resolution, particle identification and standalone muon measurement

CMS Emphasis on electron/photon and tracking (muon) resolution

Both: excellent hermeticity and forward acceptance

Trigger

Only a small fraction of events can be saved and processed with available CPU and disk space.

Trigger system identifies interesting events in two to three steps:

- Level-1: hardware-based trigger using specially designed electronics, data stored in pipeline on detector
- High-level: software-based using large computing farms, fast algorithms and/or algorithms close to offline reconstruction

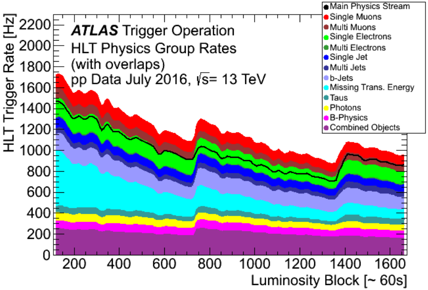

Dedicated trigger chains for different types of objects (leptons, photons, jets, ... often combining different objects in the high-level trigger)

Higgs physics

The Standard Model and the Higgs boson

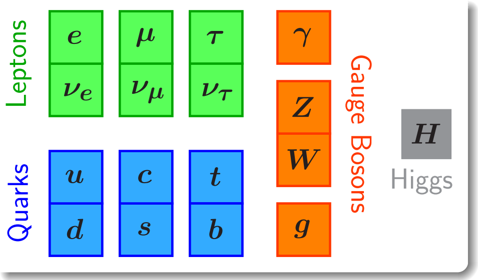

SM describes known elementary particles and their interactions

Local gauge invariance does not allow explicit mass terms in the Lagrangian – but experiment shows W and Z to have mass

- Elementary particles acquire mass through the Higgs (BEH) mechanism by interacting with the Higgs field
  - ⋆ Introduced 1964 by Brout, Englert, Higgs, Hagen, and Kibble

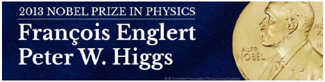

- Candidate discovered by the ATLAS and CMS experiments (2012)

What do we expect a SM Higgs boson to look like?

Introduce a scalar field with vacuum expectation value $v \neq 0$

$$\phi(x) = \begin{pmatrix} \phi^+(x) \\ \phi^0(x) \end{pmatrix} \to \langle\phi\rangle = \frac{1}{\sqrt{2}} \begin{pmatrix} 0 \\ v \end{pmatrix}$$ (unitary gauge)

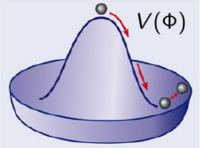

Mass terms from interaction between Higgs field and gauge bosons and fermions:

$$\mathcal{L}_\phi = (D^\mu\phi)^\dagger(D_\mu\phi) - \sum_f g_f(\bar\psi_L\phi\psi_R + \bar\psi_R\phi\psi_L) - V(\phi)$$

- Gauge boson masses $m_{W^\pm} = \frac{gv}{2}$, $m_Z = \frac{v\sqrt{g^2+g'^2}}{2}$
  - ⋆ W and Z masses determined from gauge couplings and Higgs vev
- Charged fermion masses $m_f = \frac{g_f v}{\sqrt{2}}$
  - ⋆ Not needed for electroweak symmetry breaking, but convenient to generate fermion masses

Higgs mechanism predicts the existence of a new, neutral boson: the Higgs boson, coupling to particles proportional to their mass, $J^P = 0^+$

Higgs boson production at the LHC

Gluon fusion: 48.6 pb

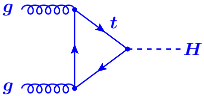

Higgs tends to have low p_T

Associated production: 2.3 pb

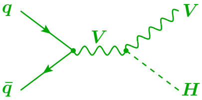

Clear signature: reconstruct W and Z in leptonic and/or hadronic decays

Vector boson fusion: 3.8 pb

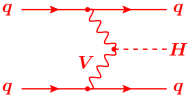

Distinct signature with 2 forward jets and little hadronic activity in between

Associated production with $t\bar{t}$: 0.5 pb

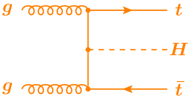

Tag presence of two top quarks

Production cross sections given at m_H =125 GeV and $\sqrt{s}$ =13 TeV

SM Higgs boson decays

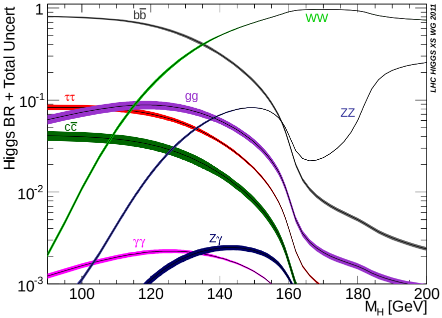

Higgs boson couples to mass

Decay branching fractions @ $m_H =$ 125 GeV

$H \to b\bar{b}$	57.7%
$H \to WW$	21.5%
$H \to \tau\tau$	6.3%
$H \to ZZ$	2.6%
$H \to \gamma\gamma$	0.23%

- Number of Higgs bosons produced in ATLAS and CMS in 2016: 4M
  - (total Higgs production cross section at 13 TeV: $\sim$55 pb)$\times$ (36 fb^{-1})$\times$(2 experiments)
- 9200 $H \to \gamma\gamma$ events
- 104000 $H \to ZZ^*$ events, but only <500 events with $Z \to ee$ and $Z \to \mu\mu$

One analysis in more detail: $H \to \gamma\gamma$

A textbook event

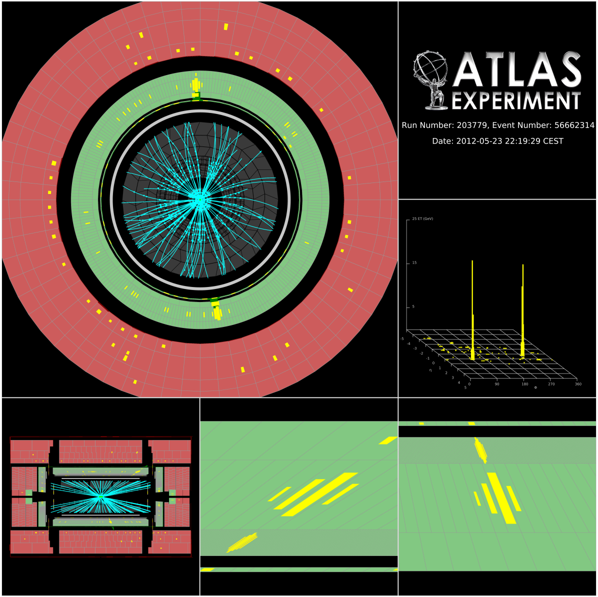

Photon reconstruction

[ATLAS-CONF-2011-161]

- Reconstruction of conversion vertices seeded from loosely selected electromagnetic clusters
  - ⋆ 2-track vertices consistent with decay of massless particle
  - ⋆ "1-track vertices" missing hits in innermost layer(s)
- Reconstructed secondary vertices (and tracks) matched to clusters in calorimeter
- Clusters without matching vertices or tracks: unconverted photons
- Reconstruction robust against pileup

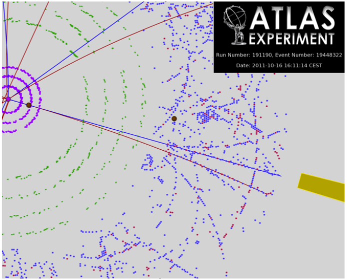

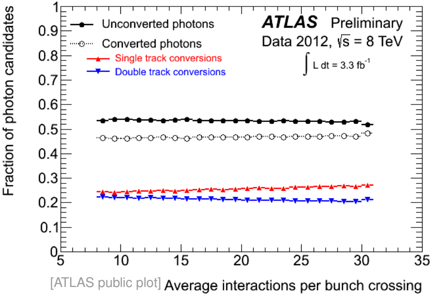

[ATLAS public plot]

Photon identification (I)

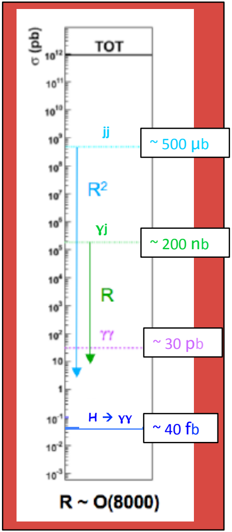

- After reconstruction, photon candidates are dominantly hadronic jets
- Need powerful jet-rejection ($\mathcal{O}(10^4)$) needed to suppress dominant hadronic background
- Fine granularity of electromagnetic calorimeter allows photon identification based on shower shape
- Generic hadronic jet leaves much broader shower than a single photon
- Tricky: jets where most of the energy is carried by a π^0

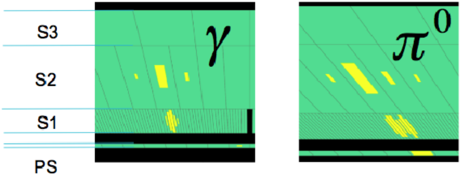

Photon identification (II)

Variables and Position

	Strips	2nd	Had.
Ratios	f_1, f_{side}	$R_\eta{}^*$, R_ϕ	$R_{Had.}{}^*$
Widths	$w_{s,3}$, $w_{s,tot}$	$w_{\eta,2}{}^*$	-
Shapes	ΔE, E_{ratio}		

* Used in PhotonLoose.

Shower Shapes

$$E_{\text{ratio}} = \frac{E^{S1}_{\text{max},1} - E^{S1}_{\text{max},2}}{E^{S1}_{\text{max},1} + E^{S1}_{\text{max},2}}$$

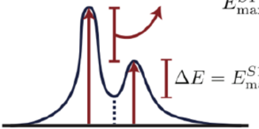

$$\Delta E = E^{S1}_{\text{max},2} - E^{S1}_{\text{min}}$$

Energy Ratios

$$R_\eta = \frac{E^{S2}_{3\times7}}{E^{S2}_{7\times7}}$$

$$R_\phi = \frac{E^{S2}_{3\times3}}{E^{S2}_{3\times7}}$$

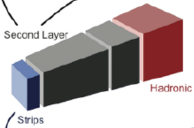

$$R_{\text{Had}} = \frac{E_T^{\text{Had}}}{E_T}$$

$$f_1 = \frac{E_{S1}}{E_{\text{Tot.}}}$$

$$f_{\text{side}} = \frac{E^{S1}_7 - E^{S1}_3}{E^{S1}_3}$$

Widths

$$w_{\eta,2} = \sqrt{\frac{\sum E_i \eta_i^2}{\sum E_i} - \left(\frac{\sum E_i \eta_i}{\sum E_i}\right)^2}$$

Width in a 3×5 (Δη×Δφ) region of cells in the second layer.

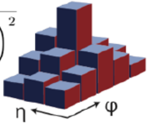

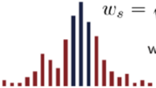

$$w_s = \sqrt{\frac{\sum E_i (i - i_{\text{max}})^2}{\sum E_i}}$$

ws3 = w_1 uses 3 strips in η; wstot is defined similarly, but uses 20 strips.

Photon identification (III)

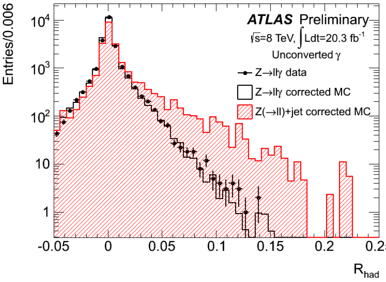

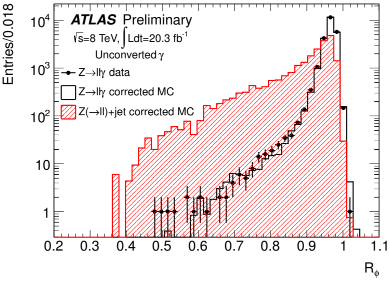

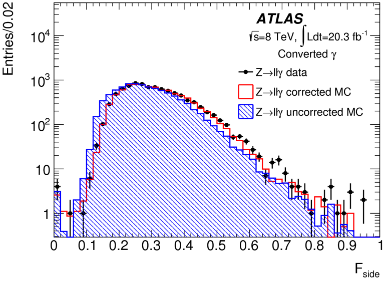

- Differences in shower shapes in data and simulation corrected ad-hoc

Photon isolation – calorimeter

- Hadronic jets deposit energy in larger area than photons
- Require photon candidates to be isolated in calorimeter
- Isolation energy computed in a cone of $\Delta R = 0.2$ around photon cluster
- Corrected for pileup effects using measured ambient energy density event-by-event

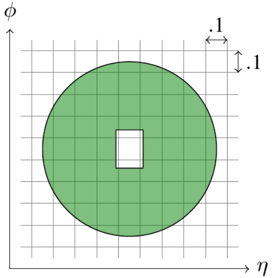

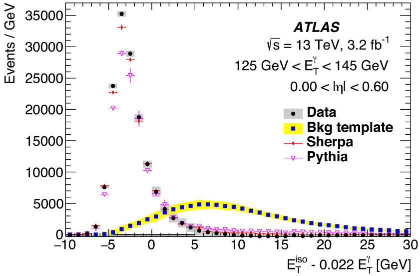

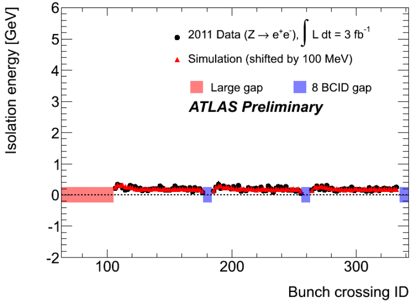

Photon isolation – tracker

- Require photon candidates to be isolated in the tracker ($\boldsymbol{\Delta R = 0.2}$)
  - ⋆ Using well-measured tracks with $\boldsymbol{p_T > 1\,\mathrm{GeV}}$
  - ⋆ Based on tracks from hard interaction primary vertex
  - ⋆ Relies on correct identification of primary vertex – see later!

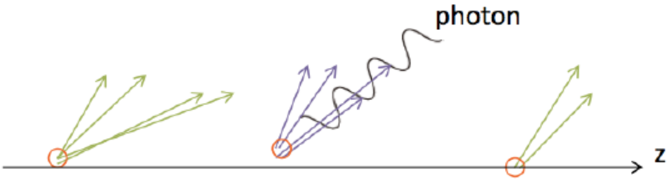

- Isolation efficiency can be measured on data using $Z \rightarrow ee$ or $Z \rightarrow \ell\ell\gamma$ events

Photon isolation – performance

- Track isolation is more pileup robust than calorimeter isolation
- Pileup correction performed by directly excluding pileup tracks vs correcting with average measured energy density
- Small isolation cones are more pileup robust than large isolation cones
- 8 TeV calorimeter isolation based on $\Delta R = 0.4$, while 13 TeV calorimeter isolation based on $\Delta R = 0.2$

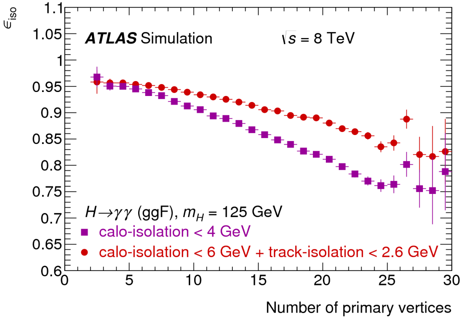

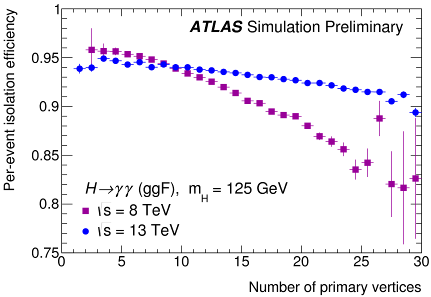

Energy calibration

From cluster energy to photon energy – in principle

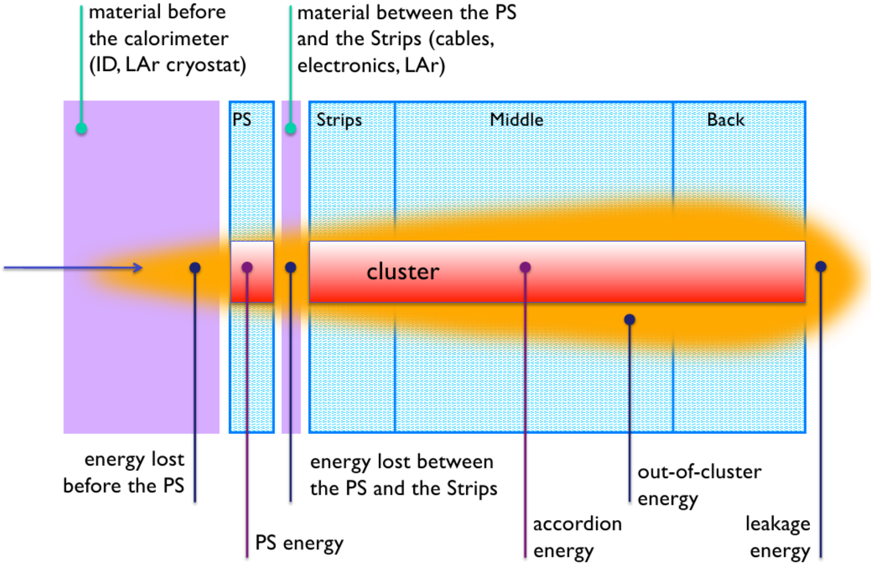

Energy calibration (II)

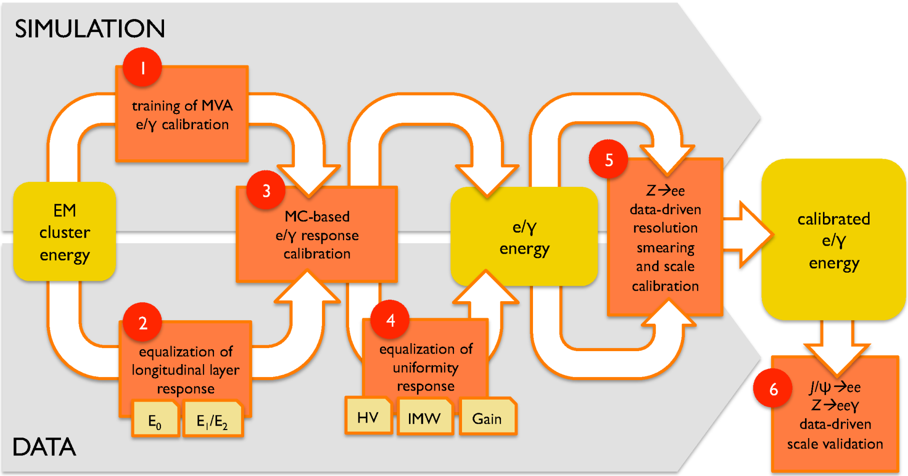

Photon pointing and primary vertex selection

$$m_{\gamma\gamma}^2 = 2E_1E_2(1 - \cos\alpha)$$

Improve photon angle measurement using neural network based on

- Photon pointing
  - ⋆ Photon direction measured from calorimeter using longitudinal segmentation
  - ⋆ Position of conversion vertex for converted photons (with Si hits)
- $\sum p_T^2$, $\sum p_T$ (over tracks) and angular balance in ϕ between tracks and diphoton system

→ Contribution of angle measurement to mass resolution negligible already without primary vertex information

→ Good primary vertex selection needed for selection of signal jets

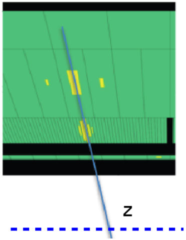

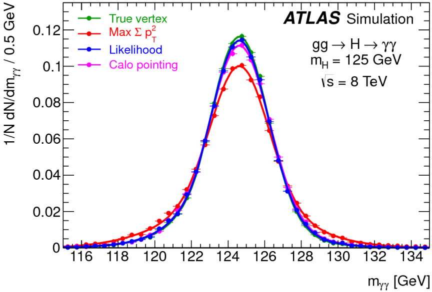

Photon pointing and primary vertex selection

$$m_{\gamma\gamma}^2 = 2E_1E_2(1 - \cos\alpha)$$

Improve photon angle measurement using neural network based on

- Photon pointing
  - ⋆ Photon direction measured from calorimeter using longitudinal segmentation
  - ⋆ Position of conversion vertex for converted photons (with Si hits)
- $\sum p_T^2, \sum p_T$ (over tracks) and angular balance in ϕ between tracks and diphoton system

→ Contribution of angle measurement to mass resolution negligible already without primary vertex information

→ Good primary vertex selection needed for selection of signal jets

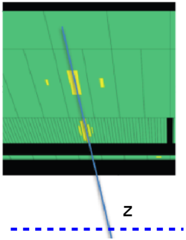

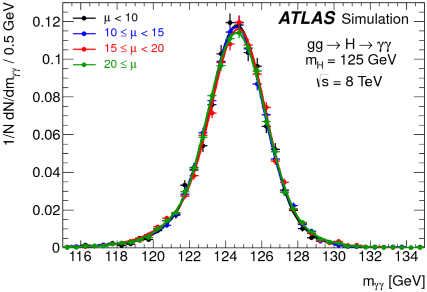

Invariant mass spectrum

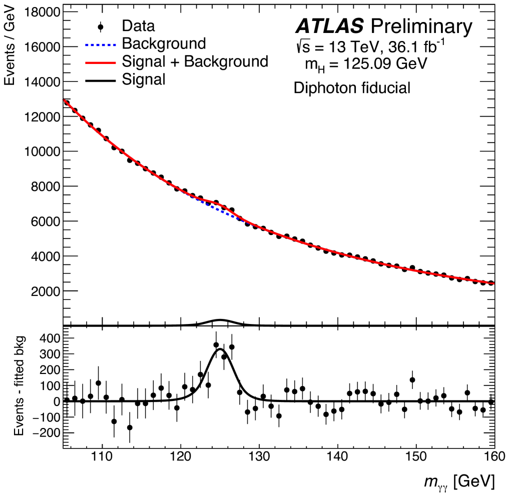

Background+signal fit, signal constrained to 125.09 GeV

Diphoton selection

Identified and isolated photons

$p_T^{\gamma 1} > 0.35 m_{\gamma\gamma}$

$p_T^{\gamma 2} > 0.25 m_{\gamma\gamma}$

Principle of a cross section measurement

Recall

$$\sigma = \frac{N}{\int \mathcal{L}\mathrm{d}t} = \frac{N_{\mathrm{meas}} - N_{\mathrm{bkgd}}}{\epsilon \cdot A \cdot \mathcal{B} \cdot \int \mathcal{L}\mathrm{d}t}$$

Experimental steps

- Estimate and subtract the background(s)
- Correct for detector acceptance, and for efficiencies
- If needed/wanted, correct for branching ratio(s)
- Determine the luminosity

Differential cross section in variable x: $\frac{\mathrm{d}\sigma}{\mathrm{d}x}$

- In practice: bin-averaged cross section $\frac{\Delta\sigma}{\Delta x}$
- Background estimation and subtraction, efficiency and acceptance corrections performed for every bin
- Requires correction of resolution effects in x: unfolding

Why cross section measurements for Higgs?

- Almost model-independent measurements of production and decay kinematics
- Measure kinematic distributions of Higgs, of associated jets, ...
- Sensitivity to Higgs production processes, QCD effects, CP, ...
- Measure inclusive cross section, and cross section in phase space enriched with VBF, and with a lepton
- Differentially in $p_T^{\gamma\gamma}$, N_{jet}, p_T^{jet}, ...

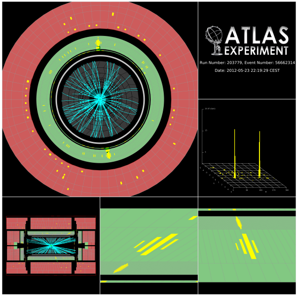

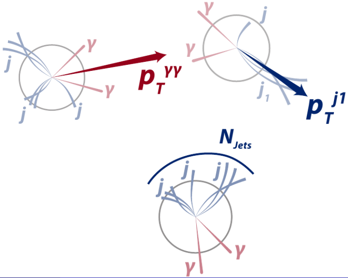

- $H \rightarrow \gamma\gamma$ and $H \rightarrow 4\ell$ decays well suited thanks to good signal invariant mass resolution $\rightarrow$ comparably “simple” analyses

Backgrounds

- Irreducible backgrounds: events with two photons, e.g.

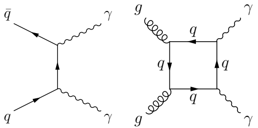

- Reducible backgrounds: events where at least one photon candidate is a misidentified jet, e.g.

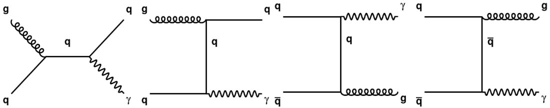

- $Z \to ee$ with the electrons misreconstructed as photons (mass tail reaches beyond $m_Z = 90\,\mathrm{GeV}$)

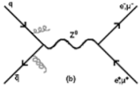

Understanding the backgrounds (I)

- Define control regions enriched in background
  - ⋆ Photon candidates that fail a given set of the shower shape cuts and/or
  - ⋆ Photon candidated that are less isolated
- Fit determines (given numbers of events in signal and control regions and photon identification and isolation efficiency)
  - ⋆ Efficiencies for jet to pass photon identification and isolation for γjet and jetjet events, separately for higher and lower p_T candidate
    - ▶ Correlation for both jets to pass isolation in jetjet events
  - ⋆ Number of $\gamma\gamma$, γjet, jetγ and jetjet events
    - ▶ $Z \rightarrow ee$ included in $\gamma\gamma$ as e look most like γ in id and isolation

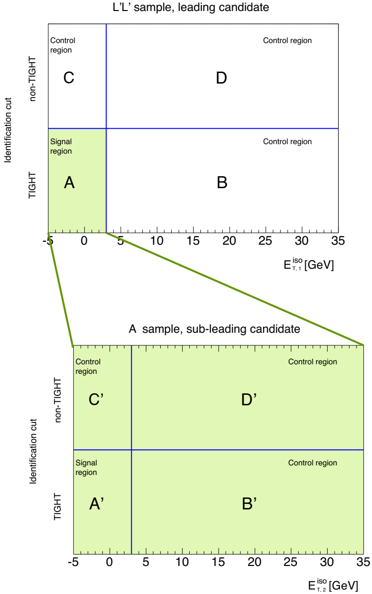

Understanding the backgrounds (II)

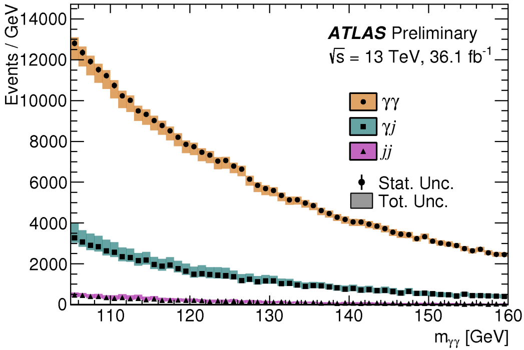

$\gamma\gamma$ $(78.7 \pm 0.2^{+1.8}_{-5.2})\%$

γjet $(18.6 \pm 0.2^{+4.2}_{-1.6})\%$

jetjet $(2.6 \pm 0.1^{+0.5}_{-0.4})\%$

Largest uncertainty: definition of control regions

- Study performed in every bin and every measured region of phase space
- Understanding of background composition not important directly to derive results, but for studies of background parametrization and photon identification

Parametrizing the signal

- Signal is extracted by a signal+background fit to $m_{\gamma\gamma}$ spectrum

- Signal is parametrized by a double-sided Crystal Ball function
  - ⋆ Gaussian with exponential tail
- SM Higgs width $4\,\mathbf{MeV}$ $(m_H = 125\,\mathbf{GeV})$
- Parameters that determine the shape are determined on simulation
- Peak position (= Higgs mass) and Gaussian width (= detector resolution) constrained within uncertainties
  - ⋆ Energy scale and resolution, and m_H
  - ⋆ Peak position unconstrained for measurement of the Higgs mass
    - ▶ To be done with Run2 data once precision energy calibration achieved
  - ⋆ Run1 Higgs mass measurement $m_H = (\mathbf{125.09 \pm 0.21(stat) \pm 0.11(syst)})\,\mathbf{GeV}$

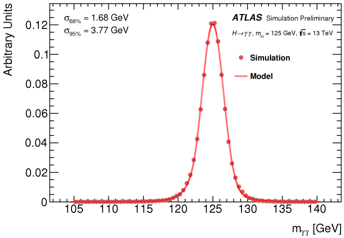

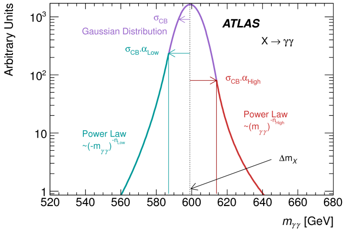

Parametrizing the backgrounds

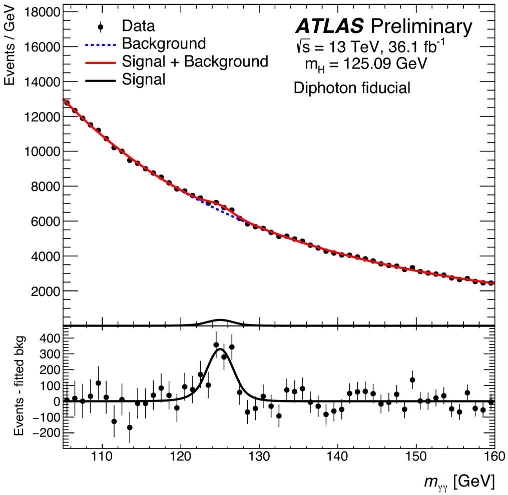

Background+signal fit, signal constrained to 125.09 GeV

Background modelled by smooth, monotonously falling function

- Polynomials (typically 3rd or 4th order)
- Exponentials of polynomials (typically 1st or 2nd order)

shape and normalization determined by the fit

Studied on high-statistics MC and chosen to give good statistical power while keeping potential biases acceptable

Potential bias accounted for as systematic uncertainty

Signal+background fit

...carried out for...

- ...all selected events → fiducial cross section
- ..after specific selections → fiducial cross section for that selection
- ...in bins of a given variable → differential spectrum

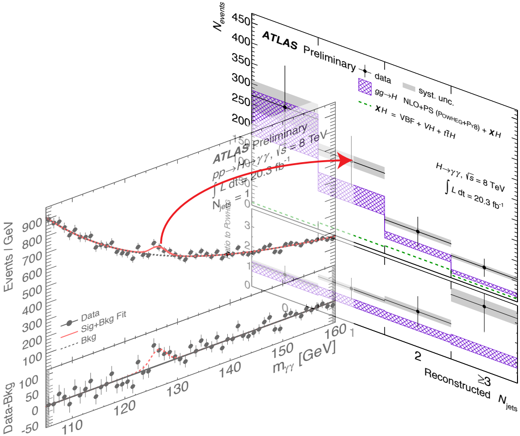

Signal+background fit

Likelihood function to be maximized

$$\mathcal{L} = \prod_i \left\{ \frac{e^{-\nu_i}}{n_i!} \prod_j^{n_i} \left[\nu_i^{\mathrm{sig}} \mathcal{F}_i^{\mathrm{sig}}(m_{\gamma\gamma}^j, \theta; m_H) + \nu_i^{\mathrm{bkg}} \mathcal{F}_i^{\mathrm{bkg}}(m_{\gamma\gamma}^j) \right] \right\} \times \prod_l G_l(\theta)$$

- for bin i and event j
- n_i number of events in bin i
- $\nu_i^{(\mathrm{sig,bkg})}$ expected number of total/signal/background events
- $\mathcal{F}_i^{(\mathrm{sig,bkg})}$ signal/background shape
- θ nuisance parameters associated with systematic uncertainties, constraint via $G_l(\theta)$
- Energy scale and resolution uncertainties, and uncertainty on m_H correlated between all bins

  $\rightarrow$ Nuisance parameters common between all bins

But wait a moment... is there a signal?

...back to summer 2012

- ⋆ Signal or statistical fluctuation of the background?

Compare compatibility of data with B-only and with S+B hypothesis with a signal scaling factor μ

Profile likelihood ratio

$$\tilde{q}_\mu = -2 \ln \frac{L(\text{data}|\mu, \hat{\hat{\theta}}_\mu)}{L(\text{data}|\hat{\mu}, \hat{\theta})}$$

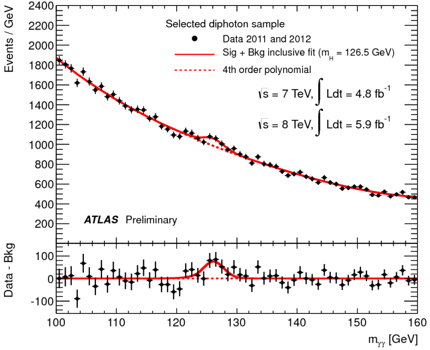

- Numerator and denominator are maximized independently
- $\hat{\hat{\theta}}_\mu$ conditional maximum given μ; $\hat{\mu}, \hat{\theta}$ corresponding to global maximum of the likelihood
- Large $\tilde{q}_\mu$ correspond to disagreement between data and hypothesis μ
- $\tilde{q}_\mu$ behaves as χ^2 for large data samples and Gaussian θ
- Denominator is only normalization term, independent of μ

Frequentist limit setting procedure

- Construct likelihood function $L(\mu, \theta)$ https://cds.cern.ch/record/1375842
- Construct test statistics $\tilde{q}_\mu$
- Perform fit to data and determine observed $\tilde{q}_{\mu,\mathrm{obs}}$ for hypothesis μ
- Generate pseudo MC to construct PDF $p_\mu(\tilde{q}_\mu|\mu, \hat{\theta}_{\mu,\mathrm{obs}})$ of $\tilde{q}_\mu$
  - ⋆ MC generation done with $\hat{\theta}_{\mu,\mathrm{obs}}$, but $\hat{\theta}_\mu$ allowed to float in the fits
- Determine the observed p-value for hypothesis μ:
  $P(\mu) = \int_{\tilde{q}_{\mu,\mathrm{obs}}}^{\infty} p_\mu(\tilde{q}_\mu|\mu, \hat{\theta}_{\mu,\mathrm{obs}})\mathrm{d}\tilde{q}_\mu$
- Perform "discovery" test by computing $P(\mu = 0)$
- Find the 95% upper bound $\mu = \mu_{95,\mathrm{obs}}$ for which $P(\mu) = 0.05$
  - ⋆ To be conservative and to avoid that upward fluctuations of the background contribute to the p-value, LHC experiments compute upper limit from $P_{\mathrm{CL}_s}(\mu) = P(\mu)/P(0) = 0.05$
    - ▶ CL$_s$ usually over-covers, so less than 5% of repeated experiments would lie outside the given bound

For complex fits pseudo-MC procedure can be very CPU intensive. Asymptotic formulae exist for cases with enough events. https://arxiv.org/abs/1007.1727

Maximum deviation from background-only expectation at $m_H = 126.5\,\mathrm{GeV}$

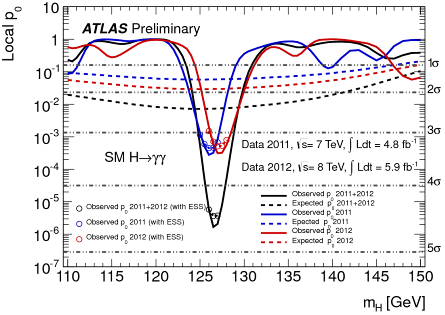

- Local significance 4.5 σ (expected 2.4 σ)
- Global significance 3.6 σ
- Need to take into account “look-elsewhere effect”: probability for a fluctuation somewhere in the studied mass range larger than for a given mass

- Require 5 σ for discovery ($p = 2.9 \cdot 10^{-7}$)
  - ⋆ Reached at ICHEP in combination with $H \to ZZ^* \to 4\ell$

Back to the measurements: Measured signal yield

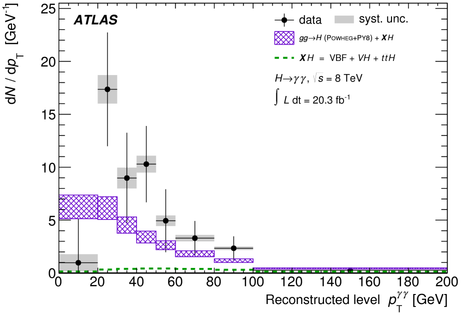

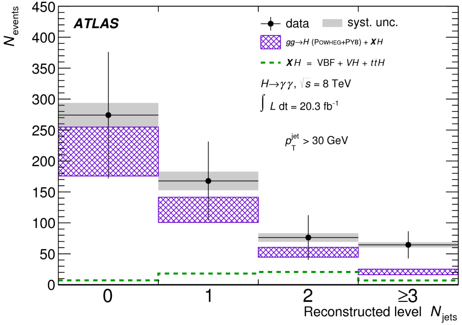

- First part achieved:

$$\frac{\mathrm{d}\sigma}{\mathrm{d}x} = \frac{N_{\mathrm{meas}} - N_{\mathrm{bkgd}}}{\epsilon \cdot A \cdot \mathcal{B} \cdot \mathrm{d}x \cdot \int \mathcal{L}\mathrm{d}t}$$

- ..although not quite...

Not mentioned so far: resolution corrections/unfolding

- $A_{ij}x_j = b_i$ (b – measured, x – true)
- Detector response matrix A encodes resolution (can also include efficiency and acceptance)
  - ⋆ A_{ij} = Probability for event in true bin j to be reconstructed in reco bin i
  - ⋆ A_{ij} is largely model independent, although there could be caveats in some cases
- "Naive" matrix inversion: $x = A^{-1}b$
  - ⋆ Unfolded spectrum x usually dominated by statistical fluctuations
    - ▶ Statistical fluctuations in measured spectrum get amplified
    - ▶ Nice explanation of this effect `here`
  - ⋆ Unbiased estimator with smallest possible variance (typically see large negative correlations between adjacent bins)

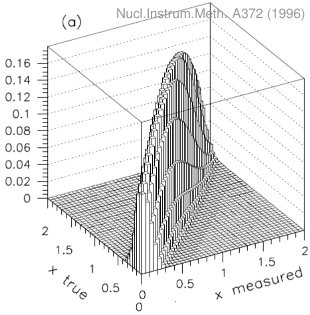

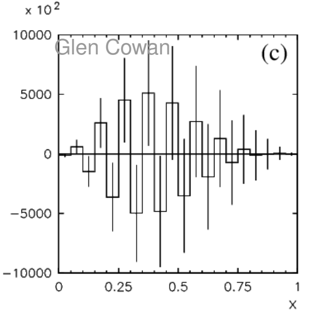

Unfolding methods – a few general words

- Most unfolding methods (effectively) invert the detector response matrix in one or another way
- Statistical fluctuations can be dampened by regularization methods that employ á priori knowledge about the distribution
  - ⋆ Widely used: curvature regularization, i.e. adding a constraint on the curvature of the unfolded distribution, making use of the fact that (most) physical distributions are smooth
- Common methods: Iterative Bayesian unfolding, Likelihood or χ^2 fit, Singular Value Decomposition based unfolding (SVD), Iterative dynamically stabilized unfolding (IDS)
- In all cases need to carefully check for biases introduced by the procedure
- Very simple method used here: correction factors

$$C_i = \frac{\text{Number of events generated in bin } i}{\text{Number of events reconstructed in bin } i}$$

Back to the analysis: efficiency corrections

- Efficiency of the reconstruction and selection

$$\epsilon = \frac{\textbf{Number of events reconstructed and selected}}{\textbf{Number of signal events in the kinematic range}}$$

Main contributions to inefficiencies in $H \to \gamma\gamma$

- photon identification
- photon isolation
- diphoton trigger

Efficiencies are measured in control samples

- Sometimes, efficiencies are determined from simulations
  - ⋆ Requires good simulation of detector and/or physics process

Photon id efficiency measurements

Radiative Z decays: $Z \to \ell\ell\gamma$

- Select two well-identified electrons or muons with 40 GeV $< m_{\ell\ell} < 83$ GeV
- and one isolated photon such that 83 GeV $< m_{\ell\ell\gamma} < 100$ GeV
- E_T^γ of 10-80 GeV
- Very high photon purity
  - ⋆ $\sim$ 90% (10-15 GeV)
  - ⋆ $\geq$ 98% ($>$ 15 GeV)
- Measured efficiencies are combined with measurements from other methods
- Analysis applies data/MC ratio as correction to simulation

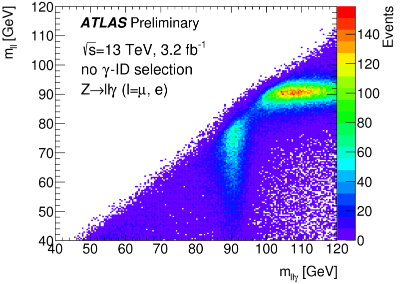

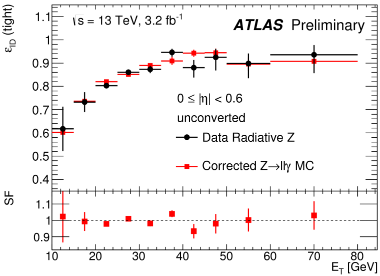

Acceptance corrections (I)

- Acceptance of the kinematic selection

$$A = \frac{\text{Number of signal events in the kinematic range}}{\text{Number of all signal events}}$$

- Experimentally accessible kinematic region is limited
  - ⋆ Small E_T photons not used due to large backgrounds
  - ⋆ Detector acceptance limited in η
- Need to use theoretical predictions to extrapolate
  - ⋆ Usually in the form of simulations
  - ⋆ Introduced dependence on theoretical predictions and their uncertainties
- Unfold to a fiducial region defined by photons (and jets) to minimize acceptance corrections
  - ⋆ $p_T^{\gamma 1(\gamma 2)} >$ 0.35 (0.25) $m_{\gamma\gamma}$, $|\eta^{\gamma 1,2}| <$ 2.37
  - ⋆ $p_T^{\text{iso}} <$ 0.05 p_T^{γ} with $p_T^{\text{iso}} \sum p_T$ of all charged particles with $p_T >$ 1 GeV within $\Delta R =$ 0.2 around photon
  - ⋆ $p_T^j >$ 30 GeV, $|y^j| <$ 4.4

Acceptance corrections (II)

Correcting from fiducial region to the full phase space would be a sizeable correction

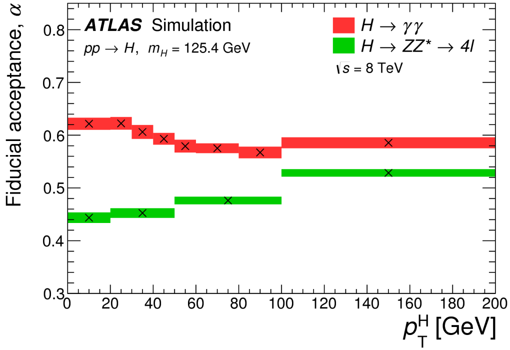

- ...of course this means that theoretical predictions will have to be done for the same fiducial region
- where not available (yet), correction factors are derived from simulation

Uncertainties

- Statistical uncertainties due to finite number of events
  - ⋆ In $H \to \gamma\gamma$, statistical uncertainties dominated by statistical uncertainties (fluctuations) in the background

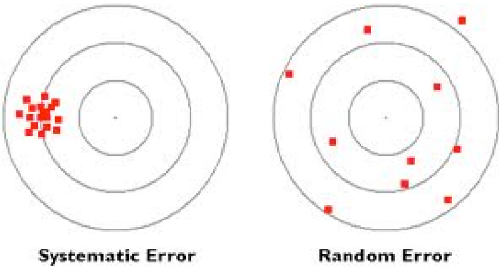

- Systematic uncertainties related to analysis inputs, procedure, ...
  - ⋆ Understanding of detector and reconstruction
  - ⋆ Understanding of backgrounds
  - ⋆ ...

- Evaluation of systematic uncertainties usually requires dedicated study for each of the possible systematic uncertainties

Uncertainties (non-differential measurement)

Source	Diphoton
Fit (stat.)	17%
Fit (syst.)	6%
Photon efficiency	1.8%
Jet energy scale/resolution	-
b-jet flavour tagging	-
Lepton selection	-
Pileup	1.1%
Theoretical modeling	4.2%
Luminosity	3.2%

- Fit (stat.) statistical uncertainty, including contributions from floating the background parameters
- Fit (syst.) uncertainties on energy scale and resolution and background parametrization
- All others uncertainties on efficiency, acceptance and resolution corrections
  - ⋆ Theoretical modelling: Higgs production cross sections, Higgs kinematics, multiple parton interactions

Fiducial cross section measurement

Fiducial cross section with fiducial region defined by photon p_T, η, and isolation

$$\sigma_{\mathrm{fid}} = 54.7 \pm 9.1\,(\mathrm{stat.}) \pm 4.5\,(\mathrm{syst})\,\mathrm{fb}$$

- Compared to theoretical predictions 63.5 ± 2.4 fb
  - ⋆ $gg \to H$ N^{3}LO precision for total cross section, corrected for fiducial acceptance (with NNLOPS, with NNLO precision for total cross section) and $H \to \gamma\gamma$ branching ratio
  - ⋆ VBF, VH, $t\bar{t}H$, ...: simulation samples reweighted to improved predictions for total cross sections
- Agreement with predictions to $1\,\sigma$

Differential cross section measurements

$p_T^{\gamma\gamma}$ $|y^{\gamma\gamma}|$ $|\cos\theta^*|$

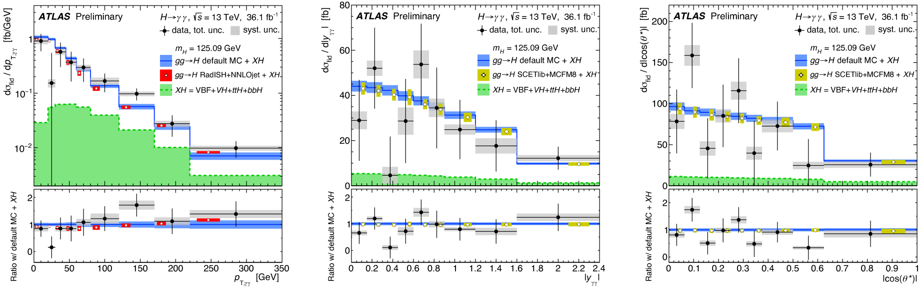

- Differential measurements presently dominated by statistical uncertainties
- Compared to MC predictions (NNLOPS for $gg \to H$, rescaled simulation for the other production processes)
  - ⋆ In addition, analytical predictions at higher order for $gg \to H$
- No significant disagreements between data and predictions within current uncertainties

Intermediate summary

Topics from today

- Overview LHC, proton collisions, and the experiments
- The Higgs boson in the SM
- A close look at the $H \to \gamma\gamma$ analysis: analysis techniques

Topics for tomorrow

- Overview of Higgs measurements and searches (in other decay channels) and combined results

Extras

Measurement of the luminosity (I)

$$\mathcal{L} = \frac{\mu n_{\mathrm{bunch}} f}{\sigma_{\mathrm{inel}}} = \frac{\mu_{\mathrm{eff}} n_{\mathrm{bunch}} f}{\sigma_{\mathrm{eff}}}$$

- μ inelastic interactions per bunch crossing
- μ_{eff} measured number of interactions per bunch crossing
- σ_{eff} effective cross section, needs to be calibrated

Luminosity monitoring algorithms

- Event counting: dedicated lumi monitor (LUCID), beam conditions monitor (BCM) (“How many bunch crossings see an event?”)
  - ⋆ Count fraction of bunch crossings without events
  - ⋆ $\mathcal{L}$ is monotonic (non-linear) function of the event rate
- Track (+primary vertex) counting: tracking detectors
- Flux counting: currents in the calorimeters

Measurement of the luminosity (II)

- Measure visible interaction rate μ_{eff} as a function of beam separation δ in beam profile scans

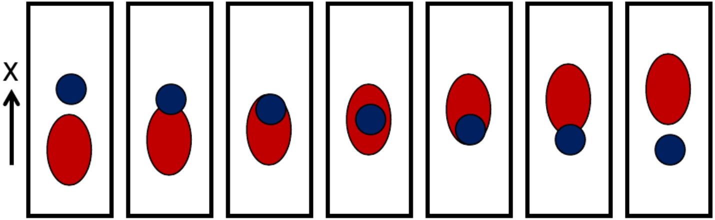

Measurement of the luminosity (II)

- Measure visible interaction rate μ_{eff} as a function of beam separation δ in beam profile scans

- Measured reference luminosity
$$\mathcal{L} = \frac{N_p^2 n_{\mathrm{bunch}} f}{2\pi \Sigma_x \Sigma_y}$$
with $\Sigma_{x,y}$ from the scan curve

- Allows direct calibration of the effective cross section σ_{eff} (for each luminosity detector/algorithm)

$$\underbrace{\boxed{\sigma_{\mathrm{eff}}}}_{\text{effective cross-section}} = \underbrace{\boxed{\mu_{\mathrm{eff}}^{\mathrm{peak}}}}_{\text{peak rate}} \frac{2\pi \overbrace{\boxed{\Sigma_x \Sigma_y}}^{\text{scan widths}}}{\underbrace{\boxed{n_1 n_2}}_{\text{bunch populations}}}$$

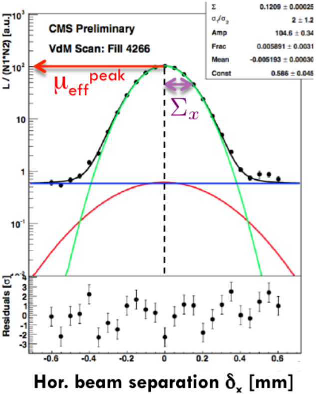

- Assumption: can factorize into scan in x and y (not completely true)

Measurement of the luminosity (II)

σ_{eff} measured in 2011 in LUCID (two different scans)

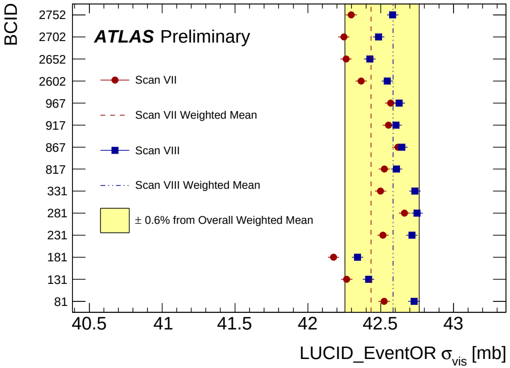

- Yellow band: uncertainty assigned from variations between scans and BCID
- Typical uncertainty on luminosity measurement 2-3%

Aside: implication of running at lower $\sqrt{s}$ in 2010-2012

- Lower $\sqrt{s} \rightarrow$ need larger x to have the same available energy

$\rightarrow$ Production of high-mass objects more difficult at lower $\sqrt{s}$

$\rightarrow$ More luminosity needed for discovery of new particles

  - ⋆ In particular for gg induced processes (like Higgs production)
  - ⋆ Relative behavior of signal and background processes also important

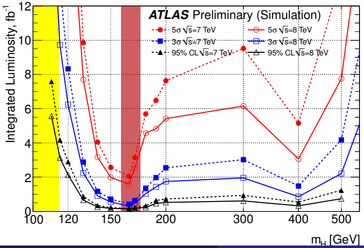

Ratio of parton luminosities at 7/14 TeV (from James Stirling)

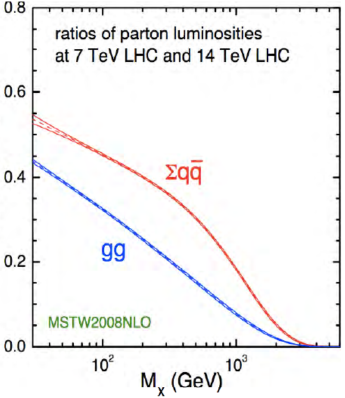

Photon reconstruction

- $\sim$ 40% of photons convert before reaching the calorimeter
- Efficient reconstruction of converted photons needed for dedicated
  - ⋆ photon energy calibration
  - ⋆ photon identification

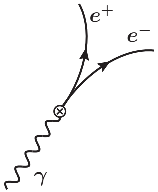

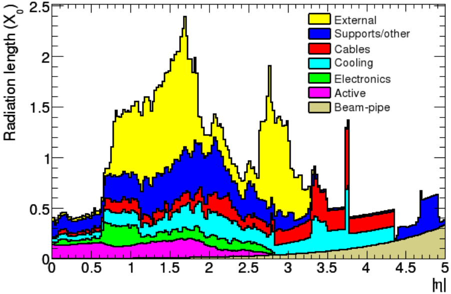

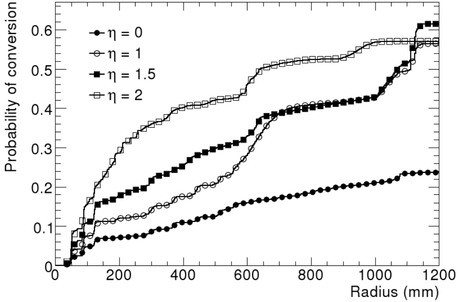

Photon identification (IV)

- Selection cuts tuned separately for converted and unconverted photons
- Aims: high efficiency for true photons, good rejection against background, as much as possible independent of pileup
- Cut values do not depend on E_T, but showers become narrower at higher E_T
  - ⋆ Less jet background at high E_T

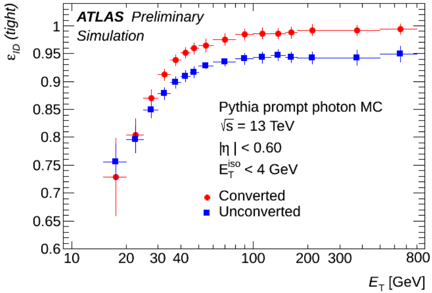

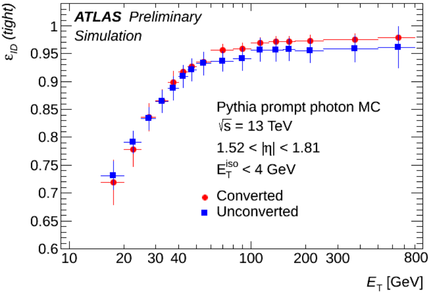

Invariant mass resolution – CMS vs ATLAS

Calorimeter resolution

- CMS crystal calorimeter with excellent intrinsic resolution

$$\frac{\sigma_E}{E} = \frac{2.8\%}{\sqrt{E}} \oplus \frac{0.12}{E} \oplus 0.3\%$$

vs ATLAS

$$\frac{\sigma_E}{E} = \frac{10\%}{\sqrt{E}} \oplus 0.7\%$$

⇒ Narrower core of resolution function in CMS compared to ATLAS, e.g. best resolution event category

- ⋆ CMS 1.18 GeV
- ⋆ ATLAS 1.39 GeV

Primary vertex selection

- ATLAS longitudinally segmented calorimeter allows for pileup-independent input to primary vertex selection
  - ⋆ CMS primary vertex selection relies entirely on tracker
- ATLAS resolution function less affected by long non-Gaussian tails arising from wrong primary vertex choice

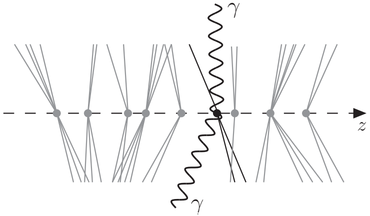

Differential cross section measurements (II)

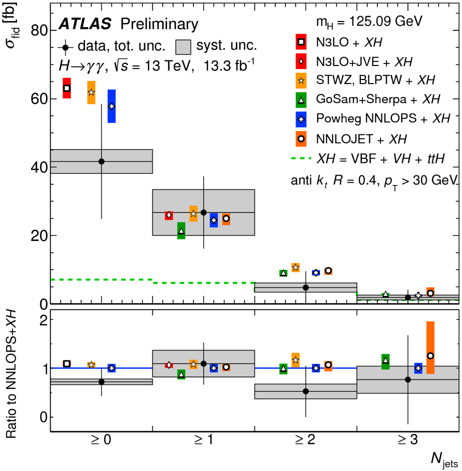

Inclusive jet cross sections (cross section for events with $\geq N$ jets) compared to a variety of theoretical predictions

- Analytical predictions for $gg \to H$ (e.g. N^{3}LO, STWZ/BLPTW)
- MC predictions (e.g. Powheg NNLOPS)